Network Reconfiguration and Distributed Energy Resource Scheduling for Improved Distribution System Resilience

Qingxin Shi[1], Fangxing Li[1], Mohammed Olama[2], Jin Dong[3], Yaosuo Xue[4], Michael Starke[4], Chris Winstead[2], and Teja Kuruganti[2]

[1]: Department of Electrical Eng. & Computer Science, University of Tennessee, Knoxville, TN, USA.

[2]: Computational Sciences & Eng. Division, Oak Ridge National Laboratory, Oak Ridge, TN, USA.

[3]: Energy & Transportation Science Division, Oak Ridge National Laboratory, Oak Ridge, TN, USA.

[4]: Electrical & Electronics Sys. Res. Division, Oak Ridge National Laboratory, Oak Ridge, TN, USA.

[*]: Corresponding author. Email: fli6@utk.edu.

Abstract - **Electric utility companies work to restore as much load as possible after power outages caused by extreme weather events. In this paper, an outage management strategy is proposed to enhance distribution system resilience through network reconfiguration and distributed energy resources (DERs) scheduling. After a line fault, the proposed algorithm can identify radial network topology based on the rank of the incidence matrix. The reconfiguration is implemented by switching tie lines and sectionalizing lines. With the new network topology, an optimal DER scheduling problem is solved to minimize the accumulative cost for dispatchable DER operation and load reduction. Finally, the optimal topology that minimizes the accumulative cost is selected from all radial topologies. The computational workload is relatively low because only linear programming needs to be solved. Using the case studies of the IEEE 69-bus and IEEE 123-bus**

This material is based upon work supported by the U.S. Department of Energy (DOE), Grid Modernization Laboratory Consortium (GMLC), DOE Office of Electricity, and Building Technologies Office. This manuscript has been authored by UT-Battelle, LLC under Contract No. DE-AC05-00OR22725 with the US Department of Energy.

systems, we consider the worst-case scenarios in which faults occur in the upstream feeder. The simulation results demonstrate that the proposed strategy allows for a relatively high percentage of the load to remain in service after line faults. Compared to microgrid-formation approaches, the proposed strategy has advantage when being applied to those distribution systems with several normally-open tie lines and low DER penetration.

Key words - Resilience, distribution system, line fault, topology reconfiguration, photovoltaic (PV) systems, distributed energy resources (DERs), microgrid.

1. Introduction

Power system resilience is an important criterion to assess the ability of a system to adapt and recover from significant power outages caused by accidents, deliberate attacks, or natural disasters [1]. Power outages in distribution systems have resulted in significant economic losses in recent years. For example, between 2003 and 2012, 679 power outages, each affecting at least 50,000 customers, occurred due to weather events in the U.S. [2]. Such severe disturbances may cause multiple line faults, which may take several hours and even more than one day to repair. During this period, electric utilities desire to serve as much load as possible and to minimize the penalty cost for load shedding, which is a critical measure of distribution system resilience [3]. There are three major approaches to enhance the resilience. The first is hardening distribution poles in critical lines so that they are less likely to be broken in extreme weather events [3]-[5]. The second is to build more normally-open tie lines. If line faults occur and some feeders are islanded, the system operator will close the tie lines to restore the loads at islanded feeders. This is called network reconfiguration [6]-[7]. The third is to increase the penetration of distributed energy resources (DERs), which include diesel engines or gas-based micro-turbines (MTs), photovoltaic (PV) systems and discharging energy storage systems (ESSs) [8]-[12].

The literature has addressed the issue of enhancing resilience from various perspectives. The study in [4] proposed a tri-level model to minimize the expense of load reduction under extreme weather. Continuing that work, the authors of [3] proposed a two-stage stochastic model with hardening actions in both distribution poles and back-up distributed generators (DGs). However, the studies in [3] and [4] did not utilize the tie lines for network reconfiguration. The study in [5] proposed a tri-level defender-attacker-defender model to determine the optimal hardening plan. However, the optimization result might be too conservative because the possibility of worst-case scenario, which is selected in the second level, might be very small. In [13], an adaptive cuckoo search algorithm was applied to reconfigure the network with the objective of power loss minimization. In [14], an approach called "modified Viterbi algorithm" was adopted to optimize the system restoration schedule and improve the voltage profile. Specifically, the radial topology has been ensured via a "switching pair" operation. However, the optimal scheduling of various types of DERs was not included in [13]-[14].

In [8], the distribution system operation has been divided into normal and self-healing modes. In the self-healing mode, the on-outage part of the system has been split into self-supplied microgrids in order to minimize the number of affected customers. The authors in [9] proposed a bi-level optimal outage management framework of sharing DERs among microgrids. The authors in [10] developed a novel centralized outage management scheme to minimize the loss of load in emergency conditions, considering outage duration uncertainty. However, the study only calculated active power and voltage-related constraints were neglected. The network reconfiguration was not considered in [9]-[10], either. A dynamically-forming microgrids algorithm was proposed in [15]. After line faults, the distribution system splits into several microgrids with an objective of maximizing the restored loads in each microgrid. In [16], the authors proposed a two-stage restoration strategy, in which the first stage decides the post-restoration topology and the second stage schedules the critical load. Additionally, a framework of distribution system restoration was proposed to generate an optimal switching sequence [17]. In [18], the system reconfiguration for service restoration was formulated as a mixed-integer second-order cone programming (MISOCP) problem. The study in [19] developed a two-stage resilience enhancement method. The pre-event stage is the optimal allocation of remotely controlled switches (RCSs), while the post-event stage is the load shedding minimization based on the existing RCSs. The study in [20] proposes an hourly reconfiguration approach with optimal DER scheduling. Despite the global optimal result, the frequent switching on/off actions can degrade the life of switches. To summarize, the control strategies in [8]-[10] and in [15]-[19] serve critical loads by making good use of DERs. However, they are based on two assumptions: 1) the DER capacity is evenly located in the distribution system, and 2) the penetration of DERs is high enough to supply the nearby load, typically in the form of a number of microgrids. In contrast, if an area of the distribution system is heavily loaded but equipped with a low to moderate penetration of DERs, it is difficult to establish multiple self-supplied microgrids within this area.

Based on the above discussions, this paper proposes a novel outage management strategy (OMS) to enhance distribution system resilience, especially for low to moderate penetration of DERs. The strategy includes post-fault reconfiguration and optimal scheduling of different types of DERs, dispatchable or non-dispatchable. The innovation can be summarized as follows:

- This work targets the scenarios of low to moderate penetration of DERs. Thus, the main supply will be considered post-fault network configuration. Also, the radial network topology is modeled as a matrix-rank based constraint in the overall OMS framework, such that we can avoid conventional empirical topological search when modeling radial topology. The strategy is applicable to N-1, N-2 and N-3 contingencies, which are common in extreme weather events.
- The comprehensive post-fault optimal DER scheduling considers various resources and uncertainties in the system including dispatchable DERs (e.g., MTs), non-dispatchable DERs (e.g., photovoltaic (PV) systems), and demand response (DR). As such, the system can be optimally configured and dispatched to provide service during emergency as long as possible. The reason for

optimal DER dispatch is that the resources during extreme events are limited, so we must optimally utilize them and ensure the supply of electricity to last as long as possible.

The remaining parts of the paper are organized as follows. Section 2 describes the operational characteristics of distribution systems. Section 3 proposes the optimal OMS, which consists of system radial topology constraints and power flow constraints. In particular, an efficient topology selection method is proposed for network reconfiguration. Section 4 introduces an empirical model to evaluate the severity of damages caused by extreme weather. Section 5 verifies the proposed method through case studies of multiple representative scenarios. Section 6 concludes the paper and introduces directions for future research.

2. Distribution System Operation Characteristics

An analysis on distribution operation characteristics is the basis for formulating the OMS. A common distribution system consists of several feeders. The feeders are installed with several sectionalizing switches (SSs), which are usually closed. A normally-open tie switch (TS) connects the end bus of the feeder. The whole system is built in radial topology because protection devices are designed based on this topology. In normal operation, the whole distribution system is served by the upstream transmission system. From the industrial application aspect, several assumptions are made for the proposed optimization model:

- A distribution system is equipped with several remotely-controlled SSs. Also, the fault indicator can successfully locate the faulted line [21].
- The system may contain various types of dispatchable DERs and non-dispatchable DERs. In the discussion in this paper, we assume that the dispatchable DERs are micro-turbines (MTs) and the non-dispatchable DERs are solar PVs for simplicity. Other types of DERs can be similarly included.
- Since the operation cost of MTs is usually higher than the price of buying electricity from the

upstream system, MTs are started only when line outages occur. PV systems always operate at the maximal power point (MPP) whether in normal or outage conditions. The forecast error of hourly-average solar irradiance is neglected. Besides, solar irradiance is identical throughout the distribution system. The PV operating cost is zero. The MTs and PV systems operate under the unity power factor.

- The upstream transmission system can operate normally in extreme weather. This assumption is based on the historical data that distribution systems contribute to 90% of the unscheduled line faults in the U.S. [22]. Also, it is feasible to keep the network connected after reconfiguration. The probability of N-k contingencies will be discussed in detail in Section 4.

During extreme weather events, one or multiple parts of the feeder might be islanded due to line faults. The islanded load will be restored if connected to another feeder through a tie line [6]. The new network topology is maintained for several hours until the broken lines are successfully repaired. During this period, there are multiple feasible reconfigurations that might ensure the radial network topology. Since line overloading may occur after reconfiguration, the dispatchable DGs are started to supply the local load and some interruptible loads are turned off. Both actions have an operation cost, namely the fuel costs and reward payments for customers. Therefore, a feasible topology that causes the minimal cost is regarded as the optimal OMS.

3. Outage Management Strategy

This section introduces the formulation of the OMS to minimize the operation cost during the period of power outage. The constraints include radial-topology constraints and DER scheduling constraints.

3.1 Objective Function

Based on the analysis in Section 2, the objective function is formulated as:

$$C(\boldsymbol{G}_k) = min. \sum_{t\in\Omega_T} \Delta t \left(\sum_{i\in\Omega_G} c^G p_{i,t}^G + \sum_{i\in\Omega_L} c_i^L \Delta p_{i,t}^L \right) \tag{1}$$

where $C(\boldsymbol{G}_k)$ is total cost of the OMS with regard to the reconfiguration topology $\boldsymbol{G}_k$ that satisfies a group of radial-topology constraints; i is the index of buses, t is the index of the time slot (one hour in this study); c^G is the fuel cost of MTs, c_i^L is the reward payment for load reduction (which can be related to the value of loss of load (VOLL) or demand response payment) at bus i, $p_{i,t}^G$ is the MT power output at bus i, time t, $\Delta p_{i,t}^L$ is the load reduction at bus i, time t; Ω_T is the period of DER scheduling (or the period of power outage), Ω_G is the set of buses with MTs, and Ω_L is the set of buses with load. Eq. (1) consists of two terms: The cost of MTs operation and the payment for load curtailment. It is well known that supplying electricity to loads under extreme weather conditions is more important than reducing the cost. However, the cost in Eq. (1) is a measure of the unserved energy considering the weighting factors of different types of loads, so it does "keep the lights on."

3.2 Network Topological Constraints

The distribution system reconfiguration should always maintain a radial topology. In this study, a rank-based constraint is proposed for selecting the radial topologies.

3.1.1 Conditions for network radial structure

In a directed graph model $\boldsymbol{G}(\Omega_N, \Omega_B)$, Ω_N represents the set of nodes (buses) and Ω_B represents the set of branches (lines). Formally, a connected graph without cycles is defined as a tree. The distribution system is a tree structure, which is also called a radial structure in power systems. The depth-first-searching algorithm is used to number all of the branches and nodes [23]. The direction of the power flow in normal operating condition is regarded as the positive direction of Ω_B. The node-branch incidence matrix $\boldsymbol{E}$ of the graph $\boldsymbol{G}$ can be deduced. The elements in $\boldsymbol{E}$ are '1', '–1' or '0'. $e_{il} = 1$ if node i is the "from node" of branch l; $e_{il} = -1$ if node i is the "to node" of branch l; $e_{il} = 0$ if node i is not connected with branch l. Finally, $\boldsymbol{E}=\left[\boldsymbol{e}_1,\boldsymbol{e}_2,\cdots,\boldsymbol{e}_{NB}\right]$, where $\boldsymbol{e}_l$ is the l-th column of $\boldsymbol{E}$ and NB is the number of branches. From graph theory, we have:

Lemma 1 If $\boldsymbol{E}$ is a connected graph on n nodes, then $rank(\boldsymbol{E}) = N - 1$ [23].

Theorem 1 The number of branches in a tree with n nodes is $N - 1$. Conversely, a connected graph with N nodes and $N - 1$ branches is a tree [24].

Lemma 1 and **Theorem 1** provide the necessary and sufficient conditions for ensuring the radial structure of a network.

When line faults occur, the system operator needs to figure out the optimal reconfiguration topology that keeps the radial structure of the network. Under this topology, the cost of required MT output and load curtailment need to be minimized. Therefore, the operator may close several TSs and open several SSs so that the islanded feeder is connected to other feeders. Figure 1 shows a simple distribution network, which consists of four feeders (named as Area-1, 2, 3, 4). If a fault occurs in Area-3, there are multiple options for keeping the network in a radial structure. For example,

- Closing TS2 or TS3 so that the islanded feeder is picked up by Area-2.
- Closing TS3, TS4, and opening SS4 so that the islanded feeder is picked up by Area-2 and Area-4.

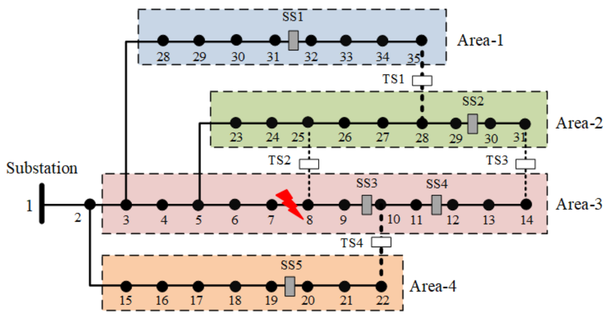

Figure 1. A feeder with multiple adjacent normal-open branches.

Based on the above analysis, the necessary and sufficient conditions to maintain the radial structure are given by (2)-(5).

$$\sum_{l \in \Omega_B} s_l = N - 1 \tag{2}$$

$$s_l = 0, \quad \forall\, l \in \Omega_{B,Fau} \tag{3}$$

$$\boldsymbol{e}'_l = \boldsymbol{e}_l \cdot s_l \quad \forall\, l \in \Omega_B, \boldsymbol{e}'_l \in \boldsymbol{E}', \boldsymbol{e}_l \in \boldsymbol{E} \tag{4}$$

$$rank\left(\boldsymbol{E}'\right) = N - 1 \tag{5}$$

where s_l is the switching state variable of line $l = (i, j)$ (1 means "close", 0 means "open"), N is the number of buses, and $\Omega_{B,Fau}$ is the set of faulted lines. Eq. (2) ensures that the total number of closed lines equals to the number of nodes (excluding the source node). Note that s_l is fixed to 1 if line l is neither installed with an RCS nor tripped. Eq. (3) means that the faulted line l is opened by the protection relay. Additionally, $\boldsymbol{E}' = \left[\boldsymbol{e}'_1, \boldsymbol{e}'_2, \cdots, \boldsymbol{e}'_{NB}\right]$ is generated by (4) after the reconfiguration. If the rank constraint (5) is satisfied, then the graph is still a connected graph.

3.2.2 Pre-defined reconfiguration topology

According to (2), if n lines are tripped, the system operator should close m TSs ($m \geq n$) and open ($m - n$) SSs. Meanwhile, the new topology should satisfy the constraint (5). The control strategy should avoid too many switching actions during the load restoration process. Therefore, we assume $0 \leq m - n \leq 1$ in this study. Before conducting the outage management, the operator needs to prepare a list of reconfiguration topologies for the anticipated fault in each area. The set of reconfiguration topologies is denoted as $\{\boldsymbol{G}_1, \boldsymbol{G}_2, \cdots, \boldsymbol{G}_{NG}\}$, where NG is the number of topologies. Each topology is represented by a vector of line switching states:

$$\boldsymbol{G}_k = \left[s_1, s_2, \cdots, s_{NB}\right] \tag{6}$$

Based on the example of Figure 1, the proposed network reconfiguration method is described as follows:

Step 1: Divide the whole network into several areas and number each of them. An area is defined as follows: Visit the buses from the substation bus to the downstream ones, if a bus (e.g. bus 2 in Figure 1) has more than one child buses (bus 3 and 15), then visit from each child bus to the end bus of this feeder (bus 14 and bus 22). Finally, all of the buses from the previous child bus to the end bus are regarded as an area (e.g., buses from 3 to 14 or buses from 15 to 22).

Step 2: Supposing that a single-line fault occurs in an area, generate a list of all reconfiguration topologies by changing the states of TSs and SSs. In practical distribution systems, there is one or two remotely-controlled SSs in one area [21]. In each topology $\boldsymbol{G}_k$, we should close at least one TS that is connected to the faulted area. Since closing two TSs (e.g., TS2 and TS4) for a single-line outage can cause a loop, we will open one SS (e.g., SS3 or SS5) within this loop. Thus, there are two possible topologies if we close TS2 and TS4. An example topology list for an Area-1 fault is shown in Table 1, which contains 8 topologies.

Step 3: Supposing that a two-line fault occurs in any two areas, generate a list of reconfigurable topologies by following a procedure similar to Step 2. An example topology list for an Area-1 and Area-3 fault is shown in Table 2. There are 10 possible topologies. Other scenarios for a two-line fault include: 1) Area-1 and Area-2, 2) Area-1 and Area-4, 3) Area-2 and Area-3, 4) Area-2 and Area-4, and 5) Area-3 and Area-4. For three-line fault, the topologies list can also be generated in a similar way. The example of topology lists is omitted here.

Table 1. Possible topology list for N-1 contingency in Area-1.

Choice	$\boldsymbol{G}_i$	TS to close	SS to open
Close one TS	$\boldsymbol{G}_1$	TS2	
	$\boldsymbol{G}_2$	TS3	
	$\boldsymbol{G}_3$	TS4	
Close two TSs	$\boldsymbol{G}_4$	TS2, TS4	SS3
	$\boldsymbol{G}_5$	TS2, TS4	SS5
	$\boldsymbol{G}_6$	TS3, TS4	SS2
	$\boldsymbol{G}_7$	TS3, TS4	SS4
	$\boldsymbol{G}_8$	TS3, TS4	SS5

Table 2. Possible topology list for N-2 contingency in Area-1 and Area-3.

Choice	$\boldsymbol{G}_i$	TS to close	SS to open
Close two TSs	$\boldsymbol{G}_1$	TS1, TS2	
	$\boldsymbol{G}_2$	TS1, TS3	

	$\boldsymbol{G}_3$	TS1, TS4	
Close three TSs	$\boldsymbol{G}_4$	TS1, TS2, TS3	SS2
	$\boldsymbol{G}_5$	TS1, TS2, TS3	SS3
	$\boldsymbol{G}_6$	TS1, TS2, TS3	SS4
	$\boldsymbol{G}_7$	TS1, TS2, TS4	SS1
	$\boldsymbol{G}_8$	TS1, TS2, TS4	SS3
	$\boldsymbol{G}_9$	TS1, TS3, TS4	SS2
	$\boldsymbol{G}_{10}$	TS1, TS3, TS4	SS4

If a line outage occurs, the fault indicator will send the line fault information to the system operator. Then, the system operator will identify in which area this fault happens and query the topology list $\{\boldsymbol{G}_1, \boldsymbol{G}_2, \cdots, \boldsymbol{G}_{NG}\}$ in the database, as shown in Figure 2. Those topologies that do not satisfy (5) are abandoned. Other topologies are selected for optimal DER scheduling and cost comparison.

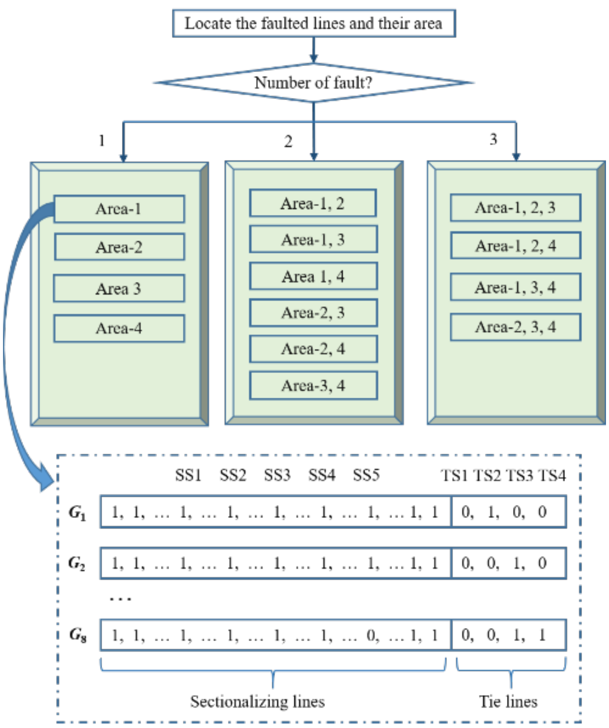

Figure 2. Database of the reconfiguration topology list.

3.3 DER Scheduling Constraints

An outage management should satisfy DER constraints and power flow constraints. Note that equations (7)-(27) are all time-dependent. Hence, we omit the expression $\forall t \in \Omega_T$ behind each equation for simplicity.

DER and load operation constraints: In this study, DERs include MTs and PV systems. The constraints of dispatchable DG units (MTs in this study) include the output power limit (7) and ramping up/down limits (8)-(9) [9]:

$$\underline{p}_i^G \le p_{i,t}^G \le \overline{p}_i^G, \ \forall i \in \Omega_G \tag{7}$$

$$p_{i,t}^G - p_{i,t-1}^G \le UR_i^{max}, \ \forall i \in \Omega_G \tag{8}$$

$$p_{i,t-1}^G - p_{i,t}^G \le DR_i^{max}, \ \forall i \in \Omega_G \tag{9}$$

where $\underline{p}_i^G / \overline{p}_i^G$ are the lower/upper limit of the MT output, UR_i^{max} and DR_i^{max} are the limit of rising/decreasing ramp. For each load type, the amount of load curtailment cannot exceed the upper bound if this load can be picked up by the tie line. The upper bound is defined by the DR contract.

$$0 \le \Delta p_{i,t}^L \le \overline{p}_{i,t}^L, \ \forall i \in \Omega_N \tag{10}$$

where $\overline{p}_{i,t}^L$ is the maximal interruptible load at bus *i*, time *t*. The system operator can control the thermostatic load for load reduction, such as turning off electric water heaters and raising the temperature setting of air conditioners [25]-[26]. The power factor is assumed to be constant. The ratio between real and reactive power (λ_i) is calculated as

$$\lambda_i = \frac{q_{i,t}^L}{p_{i,t}^L} = \frac{\sqrt{1-PF_i^2}}{PF_i}, \ \forall i \in \Omega_L \tag{11}$$

Then, the reactive power variables are replaced by the active power variables.

$$\Delta q_{i,t}^L = \lambda_i \Delta p_{i,t}^L, \ \forall i \in \Omega_L \tag{12}$$

The PV system is considered as non-dispatchable DG. In the optimization model, we assume that PV systems are working at the MPP. The power output is proportional to solar irradiance. Also, manufacturers' datasheets usually indicate the maximal power output of a PV panel when solar irradiance is 1000 W/m^2 [27]. If the solar irradiance exceeds 1000 W/m^2, the PV panel still outputs the rated power.

$$p_{i,t}^{PVmp} = min\left(Irr_t \cdot p_i^{PV,rated}, p_i^{PV,rated}\right), \ \forall i \in \Omega_{PV} \tag{13}$$

where Irr_t is the forecast average solar irradiance (kW/m^2) at time t, $p_i^{PV,rated}$ is the rated power output of the PV system, and $p_{i,t}^{PVmp}$ is the PV power output at bus i, time t, under MPP. Ω_{PV} is the set of buses with PV systems.

Nodal power injection: The power injection may include the MT output, PV system output, and load demand after curtailment. The real and reactive power injections to bus i are given by (14)-(15).

$$P_{i,t} = p_{i,t}^G + p_{i,t}^{PVmp} + 0 - \left(p_{i,t}^L - \Delta p_{i,t}^L\right), \ \forall i \in \Omega_N, i \neq 1 \tag{14}$$

$$Q_{i,t} = 0 + 0 + q_{i,t}^C - \left(q_{i,t}^L - \Delta q_{i,t}^L\right), \ \forall i \in \Omega_N, i \neq 1 \tag{15}$$

where $q_{i,t}^C$ is the reactive power generated by the shunt capacitor at bus i, time t. Note that the reactive power output of PV systems and the real power output of capacitors are denoted as zeros to make the two equations have a similar form. $q_{i,t}^C$ is proportional to the voltage squared and linearized as (16) due to the tight range of the voltage:

$$q_{i,t}^C = q_i^{C,rated} \cdot V_{i,t}^2 \approx q_i^{C,rated} \cdot \left(2V_{i,t} - 1\right), \ \forall i \in \Omega_C \tag{16}$$

where $q_i^{C,rated}$ is the rated reactive power output of the shunt capacitor at bus i, $V_{i,t}$ is the voltage magnitude of bus i, at time t, and Ω_C is the set of buses with shunt capacitors.

Linearized power flow constraints: Linearized power flow for distribution (LPF-D) can solve for the voltage magnitude and phase angle simultaneously by linear equations. LPF-D has been verified to approximate AC power flow equations with high accuracy. Compared with AC power flow, the voltage magnitude error of LPF-D is generally below 0.5% and the phase angle error of that is below 0.5 degree [28]. For all the closed lines ($s_{ij} = 1$), the LPF-D equations are:

$$P_{i,t} = \sum_{j=1, j\neq i}^{NB} P_{ij,t} = \sum_{j=1, j\neq i}^{NB} \left[B_{2\_ij}\left(\delta_{i,t} - \delta_{j,t}\right) + B_{1\_ij}\left(V_{i,t} - V_{j,t}\right)\right], \ \forall (i,j) \in \boldsymbol{G}_k, s_{ij} = 1 \tag{17}$$

$$Q_{i,t} = \sum_{j=1, j \neq i}^{NB} Q_{ij,t} = \sum_{j=1, j \neq i}^{NB} \left[-B_{1\_ij} \left(\delta_{i,t} - \delta_{j,t} \right) + B_{2\_ij} \left(V_{i,t} - V_{j,t} \right) \right], \ \forall (i,j) \in \boldsymbol{G}_k, s_{ij} = 1 \tag{18}$$

where $P_{ij,t}$ and $Q_{ij,t}$ are the real and reactive power flow of line (i, j), and $\delta_{i,t}$ is the phase angle of bus i, time t. The admittances B_{1_ij} and B_{2_ij} are given by

$$B_{1\_ij} = \frac{r_{ij}}{r_{ij}^2 + x_{ij}^2}, \ B_{2\_ij} = \frac{x_{ij}}{r_{ij}^2 + x_{ij}^2}, \ \forall (i,j) \in \boldsymbol{G}_k, s_{ij} = 1 \tag{19}$$

The substation voltage (V_{sub}) is the secondary voltage of the substation transformer and can be adjusted by the on-load tap changer. Generally, bus #1 is considered as a slack bus. Then,

$$\delta_{1,t} = 0 \tag{20}$$

$$V_{1,t} = V_{sub} \tag{21}$$

The voltage limits are assumed identical for all buses:

$$V^{min} \leq V_{i,t} \leq V^{max}, \quad \forall i \in \Omega_N, i \neq 1 \tag{22}$$

where V^{max} and V^{min} are the upper and lower voltage limits, respectively. The thermal limit of the distribution line (i, j) is expressed as S_{ij}^{max}:

$$\left(P_{ij,t} \right)^2 + \left(Q_{ij,t} \right)^2 \leq \left(S_{ij}^{max} \right)^2, \ \forall (i,j) \in \boldsymbol{G}_k, s_{ij} = 1 \tag{23}$$

According to (23), a circle in the P-Q coordinate system expresses the power flow constraint. In practical systems, $|Q_{ij,t}| \leq |P_{ij,t}|$. Thus, the nonlinear constraint (23), originally represented by a circle, can be approximated by a rectangular region as [7]:

$$-0.95 S_{ij}^{max} \leq P_{ij,t} \leq 0.95 S_{ij}^{max}, \ \forall (i,j) \in \boldsymbol{G}_k, s_{ij} = 1 \tag{24}$$

$$-0.5 S_{ij}^{max} \leq Q_{ij,t} \leq 0.5 S_{ij}^{max}, \ \forall (i,j) \in \boldsymbol{G}_k, s_{ij} = 1 \tag{25}$$

Substituting (17) and (18) into (24) and (25) gives,

$$-0.95 S_{ij}^{max} \leq B_{2\_ij} \left(\delta_{i,t} - \delta_{j,t} \right) + B_{1\_ij} \left(V_{i,t} - V_{j,t} \right) \leq 0.95 S_{ij}^{max}, \ \forall (i,j) \in \boldsymbol{G}_k, s_{ij} = 1 \tag{26}$$

$$-0.5 S_{ij}^{max} \leq -B_{1\_ij} \left(\delta_{i,t} - \delta_{j,t} \right) + B_{2\_ij} \left(V_{i,t} - V_{j,t} \right) \leq 0.5 S_{ij}^{max}, \ \forall (i,j) \in \boldsymbol{G}_k, s_{ij} = 1 \tag{27}$$

Finally, all constraints about the DER scheduling are linear or linearized and the entire optimization is a linear programming (LP) problem.

3.4 Outage Management Strategy Considering Topology Reconfiguration

To summarize, the OMS aims to determine the optimal reconfiguration topology in order to restore as much load as possible under N-K ($k \leq 3$) contingencies. The strategy is summarized in Figure 3. When a line fault occurs, the operator locates the faulted line and identifies the area which contains this line. Then, the operator finds the corresponding topology list $\{\boldsymbol{G}_1, \boldsymbol{G}_2, \cdots, \boldsymbol{G}_{NG}\}$ from the existing database, which has been presented in Figure 2. For each $\boldsymbol{G}_k$, the operator formulates the incidence matrix and calculates its rank. If the rank is N–1, then the LP of the DER scheduling is solved. $\boldsymbol{G}_k$ is eliminated if the graph is not connected or there is no feasible solution. After all of the reconfigurations are scanned, the operator selects the optimal topology that minimizes the total cost $C(\boldsymbol{G}_k)$ and saves the detailed computation result with regard to $\boldsymbol{G}_k$.

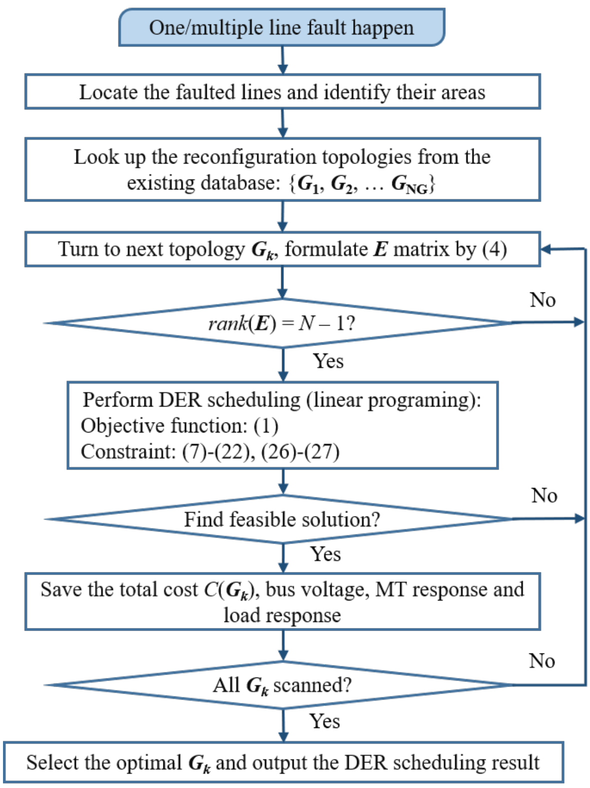

Figure 3. Flowchart of the outage management strategy.

4. Estimation of Line Fault Probability

The OMS is designed to minimize the economic loss or unsupplied energy under N-K contingencies caused by extreme weather events, such as hurricanes. It is necessary to evaluate the probability of N-K contingencies in order to identify the maximal "K" that worth considering. In practice, the overhead distribution line might be damaged by a hurricane in two ways: 1) a broken tree branch falls onto power lines, and 2) strong wind directly blows down the poles [3]-[4]. The correlation between line fault probability and wind speed can be estimated if we have sufficient historical data. In this study, a probabilistic fault model based on the "NaFIRS" database in U. K. is adopted [29]. This database recorded around 12,000 faults from 2003 to 2010 that were caused by heavy wind, including hourly-mean wind and hourly-maximum wind. During hurricanes, the hourly-maximal wind speed can be 30-38 m/s. The probability of line (i, j) fault (Pr_{ij}) is fitted by a power function of wind speed (v_m) [29]:

$$Pr_{ij} = \alpha l_{ij} (v_w)^{\beta} \tag{28}$$

Eq. (28) indicates that Pr_{ij} is proportional to the line length l_{ij}. In urban distribution systems, the constant α and β are estimated as $\alpha = 2\times10^{-17}$/km, $\beta = 9.91$. Taking a typical numerical example, if l_{ij} = 0.3km and v_m = 38m/s, then we have Pr_{ij} = 2.7%. The probability of a specified scenario s in a system is given by

$$Pr(s) = \prod_{ij\in\Omega_{B,Fau}} Pr_{ij} \cdot \prod_{ij\in\Omega_B\setminus\Omega_{B,Fau}} \left(1 - Pr_{ij}\right) \tag{29}$$

Then, the probability of all scenarios with N-K contingency is given by

$$Pr\{(N-K)\,\text{cont.}\} = \sum_{|\Omega_{B,Fau}|=K} \left[\prod_{ij\in\Omega_{B,Fau}} Pr_{ij} \cdot \prod_{ij\in\Omega_B\setminus\Omega_{B,Fau}} (1 - Pr_{ij}) \right] \tag{30}$$

where |.| means the dimension size of a set. In particular, if the fault probability of each line is identical, that is $Pr_{ij} = Pr_0$, then (30) is simplified as (31).

$$Pr\{(N-k)\,\text{cont.}\} = C_N^K \left(Pr_0\right)^K \left(1 - Pr_0\right)^{N-K} \tag{31}$$

In the IEEE 69-bus system, assume each line section has a length of 0.3 km. Then, the N-K

probability distribution under different wind speeds is obtained by (31) and shown in Figure 4. We can observe that the probability of N-K is quite small when K>3. Therefore, the OMS in this study is mainly demonstrated for N-1, N-2 and N-3 contingencies, while high-order contingencies can be similarly modeled.

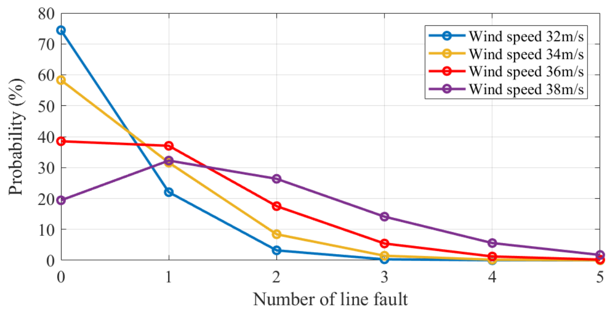

Figure 4. N-K probability distribution under different wind speeds.

5. Case Studies

During extreme weather conditions such as hurricanes, an outage may occur at any distribution line. This section presents case studies on the IEEE 69-bus system and the IEEE 123-bus system. The computational tasks are performed on a personal computer with an Intel Core i7 Processor (2.80 GHz) and 16-GB RAM, and the code is implemented via Matlab-based IBM ILOG CPLEX Optimization Studio V12.8.0.

5.1 IEEE 69-Bus System

As shown in Figure 5, the modified IEEE 69-bus system contains PV systems, MTs and shunt capacitors. There are four TSs and three critical SSs. The main parameters are listed in Table 3. In this study, we multiply each load of the original IEEE 69-bus system by 2.0 so that there is a higher possibility of voltage violation. Consequently, the robustness of the OMS can be fully tested. In addition, V^{min} is set to be 0.93 p.u. because during a contingency, restoring additional load has higher priority than maintaining a tight voltage range. The optimization time slot is one hour. The power base value is 1.0 MVA and the voltage base is 12.47kV. As shown in Figure 6, we assume that the loads follow the same load shape and PV systems follow the same solar irradiance shape. In practice, the distribution-level load can be forecast with considerable accuracy [30]-[31]. We also consider the worst case ("cloudy day") in which solar irradiance is only 30% of that on a sunny day.

In normal operating hours (1st to 12th hours), $p_{i,t}^{G}=\Delta p_{i,t}^{L}=0$. Then, the power flow is calculated by (13)-(21). At the time slot t, the total MT power output ($p_{sum,t}^{G}$) and total load reduction ($\Delta p_{sum,t}^{L}$) are calculated by (32) and (33), respectively.

$$p_{sum,t}^{G}=\sum_{i\in\Omega_G}p_{i,t}^{G} \tag{32}$$

$$\Delta p_{sum,t}^{L}=\sum_{i\in\Omega_L}\Delta p_{i,t}^{L} \tag{33}$$

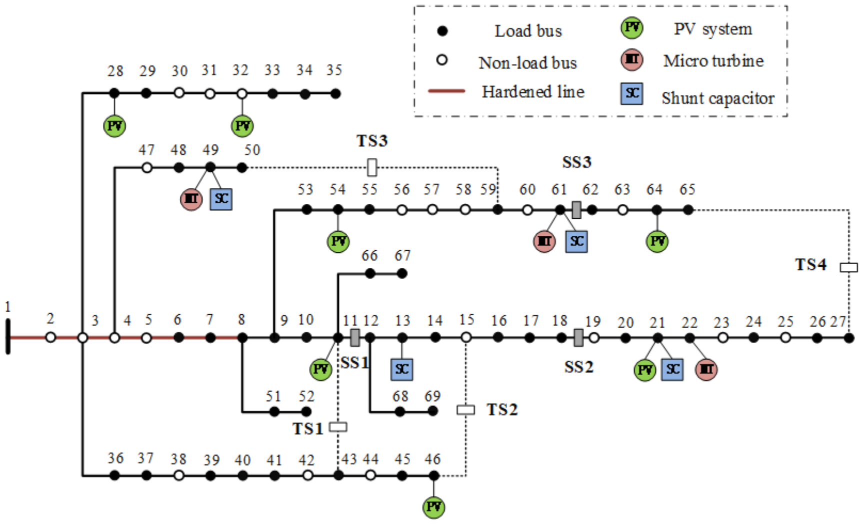

Figure 5. The IEEE 69-bus system with DERs.

Table 3. Parameters of the IEEE 69-bus system.

Class	Parameter	Value
System components	Peak load	7.58 MW + j5.39 MVar
	MT	3 devices, 1.16 MW capacity
	PV systems	7 devices, 1.20 MW capacity
	Shunt capacitors	4 devices, 1.40 MVar capacity
Cost	c^G	\$0.25/kWh
	c_i^L	\$1.2/kWh (critical load) \$0.4/kWh (non-critical load)
System voltage	V_{sub}	1.03 p.u.
	V^{max}	1.05 p.u.
	V^{min}	0.93 p.u.

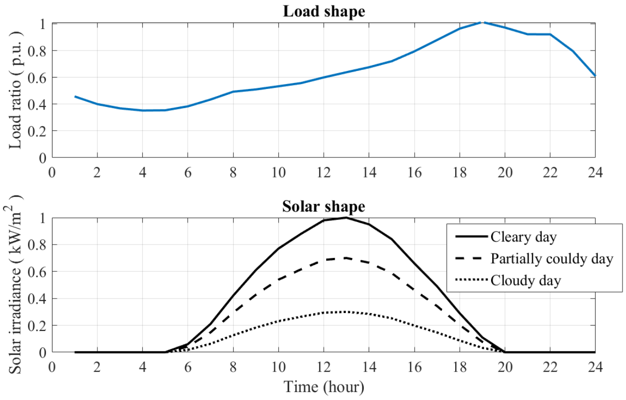

Figure 6. Load and solar profiles.

5.1.1 Scenarios of Two-Line Fault

In this subsection, we consider two severe scenarios of N–2 contingencies:

- Scenario 1: Lines 10-11 and 54-55 are tripped at 13:00.
- Scenario 2: Lines 12-13 and 47-48 are tripped at 13:00.

The topology searching result is presented in Table 4. The total computational times of Scenario 1 and Scenario 2 are 0.524 and 0.362 seconds, respectively. There are ten candidate topologies in Scenario 1 and nine candidate topologies in Scenario 2. The minimal costs for Scenarios 1 and 2 are \$4,346 and \$5,914, respectively. Some topologies (e.g., $\boldsymbol{G}_2$ and $\boldsymbol{G}_4$ in Scenario 1) are eliminated because the algorithm cannot find a feasible solution for DER scheduling. Additionally, some topologies (e.g., $\boldsymbol{G}_4$ in Scenario 2) are also eliminated by the rank constraint (5). The optimal topologies of the two scenarios are shown in Figure 7. The curves of $p^G_{sum,t}$ and $\Delta p^L_{sum,t}$ with regard to optimal topologies are presented in Figure 8. It is observed that although $p^G_{sum,t}$ and $\Delta p^L_{sum,t}$ of the two scenarios are almost equal, Scenario 2 has much higher cost than Scenario 1. The reason is that more critical loads are turned off in Scenario 2. According to Figure 8, the maximal load reduction of both scenarios occurs at the 19th hour. $\Delta p^L_{sum,19}$ is 1.203 MW in Scenario 1. If we do not consider any reconfiguration and let the MTs and PV systems supply the islanded load, $\Delta p^L_{sum,19}$ will be 3.758 MW.

Table 4. Topology selections result of Scenarios 1 & 2.

G_i	Scenario 1		Scenario 2	
	Switching action	$C(G_k)$ (\$)	Switching action	$C(G_k)$ (\$)
G_1	Close TS1 and TS3	**4346**	Close TS1 and TS3	N/C [2]
G_2	Close TS1 and TS4	N/F [1]	Close TS2 and TS3	6265
G_3	Close TS2 and TS3	**4346**	Close TS3 and TS4	8298
G_4	Close TS2 and TS4	N/F	Close TS1, TS3 and TS4, open SS1	N/C
G_5	Close TS3 and TS4	N/F	Close TS1, TS3 and TS4, open SS2	N/C
G_6	Close TS1, TS3 and TS4, open SS1	N/F	Close TS1, TS3 and TS4, open SS3	N/C
G_7	Close TS1, TS3 and TS4, open SS2	4401	Close TS2, TS3 and TS4, open SS2	6707
G_8	Close TS1, TS3 and TS4, open SS3	6435	Close TS2, TS3 and TS4, open SS3	**5914**
G_9	Close TS2, TS3 and TS4, open SS2	4401	Close TS1, TS2 and TS3, open SS1	N/C
G_{10}	Close TS2, TS3 and TS4, open SS3	6435		

[1] N/F means that this topology is radial, but there is no feasible solution of DER scheduling.

[2] N/C means that this topology is not a connected graph because $rank(\boldsymbol{E}) < 68$

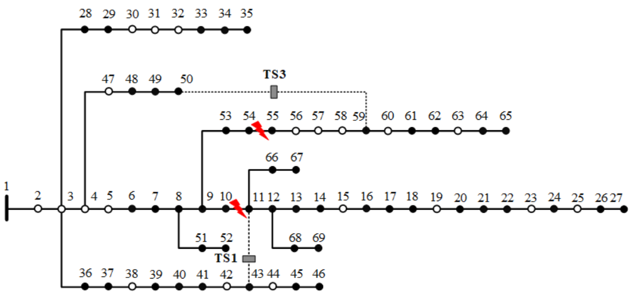

(a)

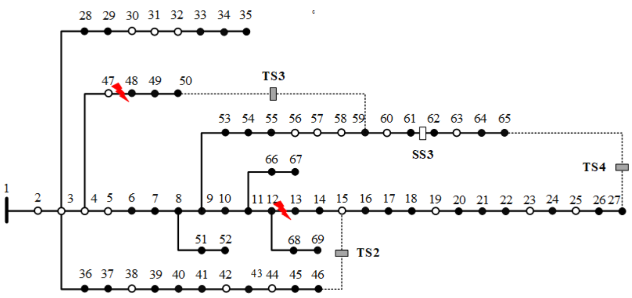

(b)

Figure 7. Optimal reconfiguration topologies: (a) Scenario 1; (b) Scenario 2.

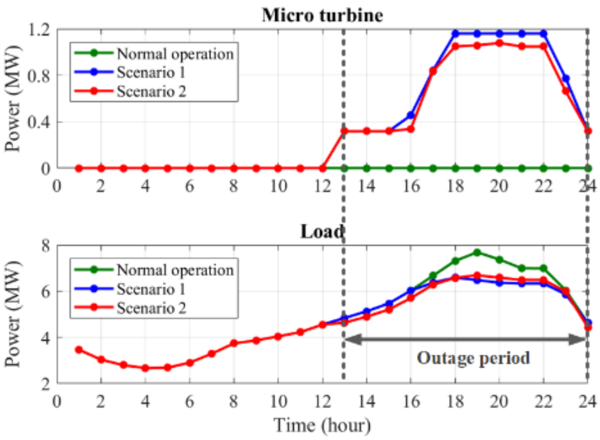

Figure 8. The total MT and load scheduling results.

The bus voltages are sorted at each time slot and presented in Figure 9. We can observe that some buses in Scenario 2 suffer low voltages (<0.95 p.u.) during peak load hours. This under-voltage problem is caused by the extremely large impedances of lines 57-58, 60-61 and 63-64 and heavy power flow through those lines. It should be noted that the low voltage problem also exists in normal operating state when loading level is high. During the outage period, serving more load has higher priority than keeping a tight voltage range. Thus, the voltage limit can be relaxed to supply more loads. Also, the operator may consider to install shunt capacitors near the heavy load buses to improve voltages. In short, when conducting the reconfiguration, the bus voltage limit can be relaxed to reduce or even eliminate the load reduction due to voltage violation.

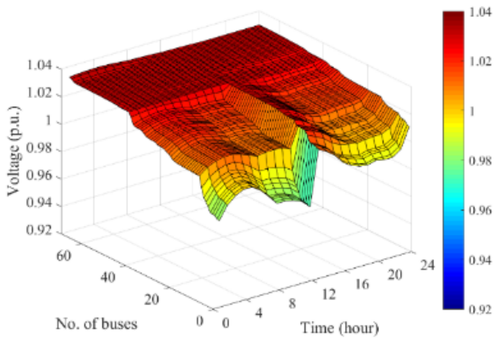

(a)

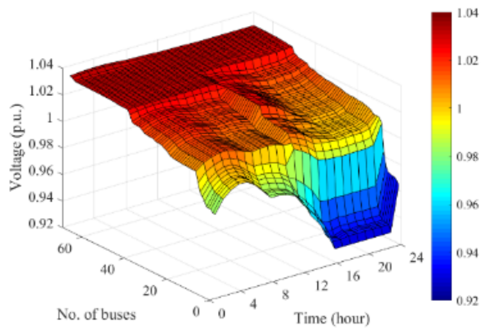

(b)

Figure 9. 3-D voltage profile: (a) Scenario 1; (b) Scenario 2.

5.1.2 Scenarios of Three-Line Fault

In this subsection, we consider two severe scenarios of N–3 contingencies:

- Scenario 3: Lines 12-13, 38-39 and 4-47 are tripped at 13:00.
- Scenario 4: Lines 36-37, 47-48 and 62-63 are tripped at 13:00.

The topology searching result is presented in Table 5. The total computational times of Scenario 3 and Scenario 4 are 0.243 and 0.278 second, respectively. There are four topologies in Scenario 3 and five topologies in Scenario 4. The minimal costs for Scenarios 3 and 4 are \$7,377 and \$5,817, respectively. Additionally, some topologies (e.g., $\boldsymbol{G}_3$ in Scenario 3) are also eliminated by the rank constraint (5). The optimal topologies of the two scenarios are presented in Figure 10. The curves of $p_{sum,t}^{G}$ and $\Delta p_{sum,t}^{L}$ with regard to optimal topologies are presented in Figure 11. According to the figure, the maximal load reduction of both scenarios occurs at the 19$^{\text{th}}$ hour. $\Delta p_{sum,19}^{L}$ is 1.354 MW in Scenario 3. If we do not consider any reconfiguration and let the MTs and PV systems supply the islanded load, $\Delta p_{sum,19}^{L}$ will be 2.814 MW. Therefore, the network reconfiguration has greatly reduced the loss of load even when the DER penetration is relatively low.

Table 5. Topology selections result of Scenarios 3 & 4.

G_i	Scenario 3		Scenario 4	
	Switching action	$C(G_k)$ ($)	Switching action	$C(G_k)$ ($)
G_1	Close TS1, TS3, and TS4	8487	Close TS1, TS3, and TS4	**5817**
G_2	Close TS2, TS3, and TS4	9432	Close TS2, TS3, and TS4	5889
G_3	Close TS1, TS2, TS3 and TS4, open SS1	N/C	Close TS1, TS2, TS3 and TS4, open SS1	6041
G_4	Close TS1, TS2, TS3 and TS4, open SS2	**7377**	Close TS1, TS2, TS3 and TS4, open SS2	N/C
G_5			Close TS1, TS2, TS3 and TS4, open SS3	N/C

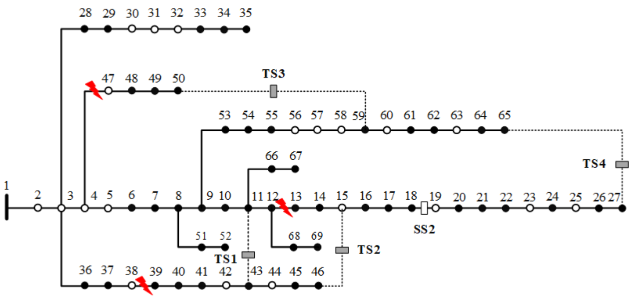

(a)

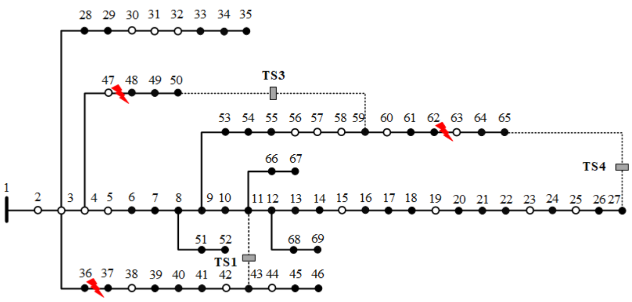

(b)

Figure 10. Optimal reconfiguration topologies: (a) Scenario 3; (b) Scenario 4.

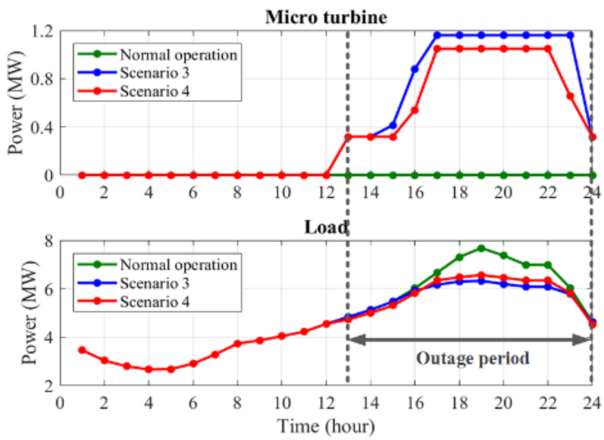

Figure 11. The total MT and load scheduling results.

The bus voltages are sorted at each time slot, as shown in Figure 12. Similar to Scenario 2, the result of Scenario 3 also indicates that some loads are turned off because of voltage constraints. Again, the bus voltage limit can be relaxed, if needed, to reduce or even eliminate the load reduction due to voltage violation.

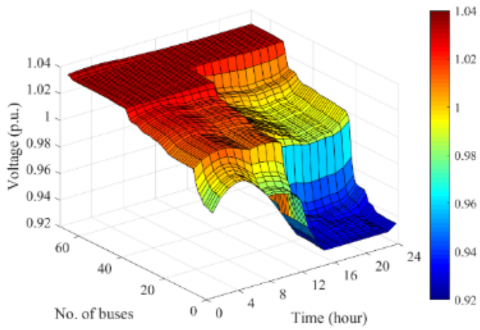

(a)

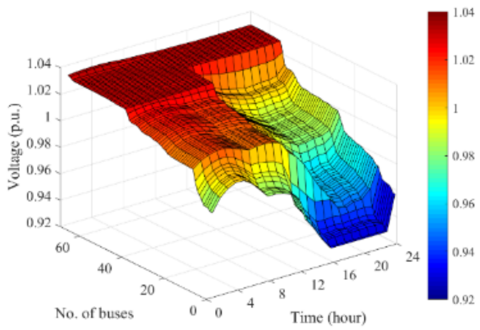

(b)

Figure 12. 3-D voltage profile: (a) Scenario 3; (b) Scenario 4.

5.2 IEEE 123-bus System

The modified single-phase IEEE 123-bus system is shown in Figure 13. The four normally-open tie lines are 29-48, 39-66, 54-94, and 115-116. The system component parameters are listed in Table 6. The DER penetration in this system is 25.20%. Other parameters such as cost, system voltage limit, wind speed and day type are the same as those in Table 3. The same sets of load and solar profiles as the 69-bus system are adopted. All faults are assumed to occur at the 10th hour and repaired at the 22nd hour. Two typical scenarios are tested:

- *Scenario 5*: Lines 13-18 and 105-108 are tripped.
- *Scenario 6*: Lines 18-21, 35-40 and 72-76 are tripped.

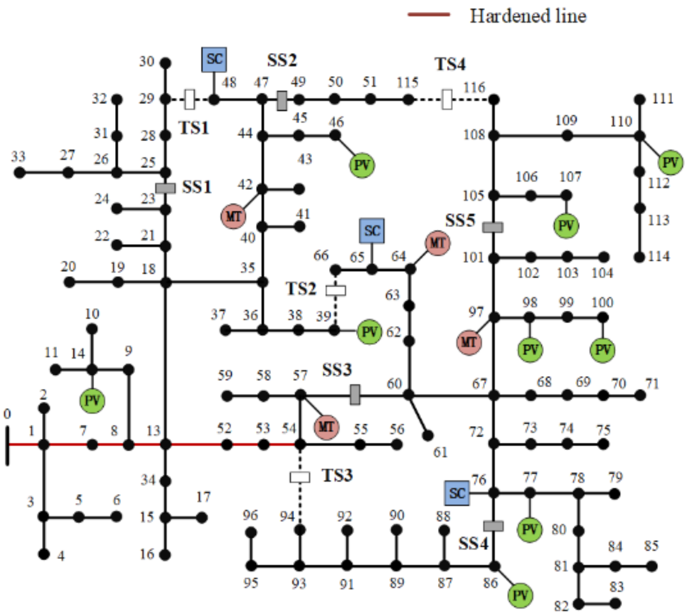

Figure 13. The IEEE 123-bus system with DERs.

Table 6. Parameters of the IEEE 123-bus system.

Parameter	Value
Load	7060kW + j 3880kvar
MT	4 devices, 660kW capacity
PV systems	9 devices, 1120kW capacity
Shunt capacitors	3 devices, 840kvar capacity

The topology searching result and the minimal cost of the two scenarios are presented in Table 7. The total computational times of Scenario 5 and Scenario 6 are 1.271 and 0.823 seconds, respectively. The curves of $p^{G}_{sum,t}$ and $\Delta p^{L}_{sum,t}$ with regard to optimal topologies are presented in Figure 14. In particular, Scenario 6 has larger load reduction because line 54-57 reaches the thermal limit after reconfiguration. In other words, the thermal limit of this “bottleneck” line determines how much load can be restored by reconfiguration. The lowest voltages of Scenario 5 and Scenario 6 are 0.982 p.u. and 0.967 p.u., respectively. The bus voltages are in a tighter range than those of the 69-bus system because there are no lines with large impedances.

Table 7. The optimal topology of Scenarios 5 & 6.

Scenario 5		Scenario 6	
Switching action	$C(\boldsymbol{G}_k)$ (\$)	Switching action	$C(\boldsymbol{G}_k)$ (\$)
Close TS2, TS3, and TS4; open SS4	3619	Close TS1, TS3, and TS4	6482

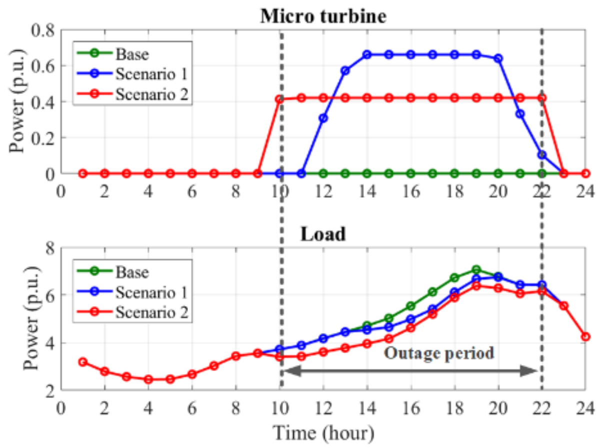

Figure 14. The total MT and load scheduling results.

6. Conclusion

A resilient distribution system means serving as much load as possible after N-K contingencies caused by natural disasters. This paper develops an OMS for the post-fault restoration of distribution systems. The OMS consists of both network reconfiguration and DER scheduling. Compared with microgrid-formation approaches that require high DER penetration, the proposed strategy has advantage when being applied to those distribution systems with several normally-open tie lines and low DER penetration.

The contributions of this paper are two-fold. First, a topology selection method is proposed to determine the optimal topology that minimizes the total outage cost. In particular, rank-based constraints are utilized to ensure the radial structure when selecting the reconfiguration topologies. Second, an optimal DER scheduling method is proposed, with the consideration of dispatchable MTs, non-dispatchable PV systems, shunt capacitors and DR. The proposed technique is validated by the case studies of multiple representative scenarios, which consider the large power outage and low solar irradiance. The results indicate that the proposed strategy can maintain a high percentage of loads in service under N–2 and N–3 contingencies, which are very common in typical hurricane days. Furthermore, the impact of load forecast errors and solar forecast errors on optimization results may be the subject of future works.

Reference

[1] M. S. Khomami, K. Jalilpoor, M. T. Kenari, M. S. Sepasian, "Bi-level network reconfiguration model to improve the resilience of distribution systems against extreme weather events," *IET Gener., Transm. & Distrib.*, vol. 13, no. 15, pp. 3302-3210, May 2019.

[2] Executive Office of the President, *Economic benefits of increasing electric grid resilience to weather outages*, Tech. Rep., 2013.

[3] S. Ma, L. Su, Z. Wang, F. Qiu, and G. Guo, "Resilience enhancement of distribution grids against extreme weather events," *IEEE Trans. Power Syst.*, vol. 33, no. 5, pp. 4842-4853, Sep. 2018.

[4] S. Ma, B. Chen, and Z. Wang, "Resilience enhancement strategy for distribution systems under extreme weather events," *IEEE Trans. Smart Grid*, vol. 9, no. 2, pp. 1442-1451, Mar. 2018.

[5] Y. Lin, Z. Bie, "Tri-level optimal hardening plan for a resilient distribution system considering reconfiguration and DG islanding," *Appl. Energ.*, vol. 210, pp. 1266-1279, Jan. 2018.

[6] C. Chen, J. Wang, and D. Ton, "Modernizing distribution system restoration to achieve grid resiliency against extreme weather events: An integrated solution," *Proceedings of the IEEE*, vol. 105, no. 7, pp. 1267-1288, Jul. 2017.

[7] T. Ding, Y. Lin, Z. Bie, and C. Chen, "A resilient microgrid formation strategy for load restoration considering master-slave distributed generators and topology reconfiguration," *Appl. Energy*, vol. 199, pp. 205-216, Aug. 2017.

[8] Z. Wang and J. Wang, "Self-Healing resilient distribution systems based on sectionalization into microgrids," *IEEE Trans. Power Syst.*, vol. 30, no. 6, pp. 3139-3149, Nov. 2015.

[9] H. Farzin, M. Fotuhi-Firuzabad, and M. Moeini-Aghtaie, "Enhancing power system resilience through hierarchical outage management in multi-microgrids," *IEEE Trans. Smart Grid*, vol. 7, no. 6, pp. 2869-2879, Nov. 2016.

[10] H. Farzin, M. Fotuhi-Firuzabad, and M. Moeini-Aghtaie, "Role of outage management strategy in reliability performance of multi-microgrid distribution systems," *IEEE Trans. Power Syst.*, vol. 33, no. 3, pp. 2359-2369, May 2018.

[11] Distributed energy resources - Technical considerations for the bulk power system, *Federal Energy Regulatory Commission* (*FERC*), Docket No. AD18-10-000, Feb. 2018.

[12] G. Zu, J. Xiao, and K. Sun, "Mathematical base and deduction of security region for distribution systems with DER," *IEEE Trans. Smart Grid*, vol. 10, no. 3, pp. 2892-2903, May 2019.

[13] T. T. Nguyen, A. V. Truong, and T. A. Phung, "A novel method based on adaptive cuckoo search for optimal network reconfiguration and distributed generation allocation in distribution network," *Int. J. Electr. Power Energ. Syst*., vol. 78, pp. 801–815, 2016.

[14] C. Yuan, M. S. Illindala, and A. S. Khalsa, "Modified Viterbi algorithm based distribution system restoration strategy for grid resiliency," *IEEE Trans. Power Del.*, vol. 32, no. 1, pp. 310-319, Feb. 2017.

[15] C. Chen, J. Wang, F. Qiu, and D. Zhao, "Resilient distribution system by microgrids formation after natural disasters," *IEEE Trans. Smart Grid*, vol. 7, no. 2, pp. 958-966, Mar. 2016.

[16] Y. Wang, Y. Xu, *et al*., "Coordinating multiple sources for service restoration to enhance resilience of distribution systems," *IEEE Trans. Smart Grid*, vol. 10, no. 5, pp. 5781-5793, Sept. 2019.

[17] B. Chen, Z. Ye, C. Chen, and J. Wang, "Toward a MILP modeling framework for distribution system restoration," *IEEE Trans. Power Syst.*, vol. 34, no. 3, pp. 1749-1760, May 2019.

[18] S. Yao, T. Zhao, P. Wang, H. Zhang, “Resilience-oriented distribution system reconfiguration for service restoration considering distributed generations,” in *2017 IEEE PES General Meeting*, Chicago, IL, Jul. 2017.

[19] J. Liu, Y. Yu, C. Qin, “Unified two-stage reconfiguration method for resilience enhancement of distribution systems,” *IET Gener., Transm. & Distrib*., vol. 13, no.9, pp. 1734-1745, Mar. 2019.

[20] E. Kianmehr, S. Nikkhah, *et al*., “A resilience-based architecture for joint distributed energy resources allocation and hourly network reconfiguration,” *IEEE Trans. Ind. Informat.*, vol. 15, no. 10, pp. 5444-5455, Feb. 2019.

[21] Distribution system automation: results from the smart grid investment grant program, Dept. of Energy, Sep. 2016. [Available] https://www.energy.gov/sites/prod/files/2016/11/f34/Distribution%20Automation%20Summary%20Report_09-29-16.pdf.

[22] R. J. Campbell, *Weather-related power outages and electric system resiliency: congressional research service*. Washington, DC, USA: Libraryof Congress, 2012.

[23] R. B. Bapat, *Graphs and matrices*, 2nd edition, Springer, 2014. pp. 14.

[24] R. Balakrishnan and K. Ranganathan, *A textbook of graph theory*, Springer, 2012. pp. 75.

[25] Q. Shi, C. Chen, A. Mammoli, and F. Li, "Estimating the profile of incentive-based demand response (IBDR) considering technical models and social-psychological factors," *IEEE Trans. Smart Grid*, vol. 11, no. 1, pp. 171-183, Jan. 2020.

[26] H. Hui, Y. Ding, and *et al*., “5G network-based internet of things for demand response in smart grid: A survey on application potential,” *Appl. Energy*, vol. 257, pp. 1-15, Jan. 2020.

[27] R. Torquato, Q. Shi, W. Xu, and W. Freitas, "A Monte Carlo simulation platform for studying low voltage residential networks," *IEEE Trans. Smart Grid*, vol. 5, no. 6, pp. 2766-2776, Nov. 2014.

[28] H. Yuan, F. Li, Y. Wei, and J. Zhu, "Novel linearized power flow and linearized OPF models for active distribution networks with application in distribution LMP," *IEEE Trans. Smart Grid*, vol. 9, no. 1, pp. 438-448, Jan. 2018.

[29] S. Dunn, S. Wilkinson, *et al*., “Fragility curves for assessing the resilience of electricity networks constructed from an extensive fault database,” *Nat. Hazards Rev*., vol. 19, no. 1, pp. 1-10, Feb. 2018.

[30] H. Jiang, *et al.*, "A short-term and high-resolution distribution system load forecasting approach using support vector regression with hybrid parameters optimization," *IEEE Trans. Smart Grid*, vol. 9, no. 4, pp. 3341-3350, Jul. 2018.

[31] M. Dong and L. S. Grumbach, "A hybrid distribution feeder long-term load forecasting method based on sequence prediction," *IEEE Trans. Smart Grid*, vol. 11, no. 1, pp. 470-482, Jan. 2020.